PHYSICAL REVIEW A **90**, 053407 (2014)

# Dynamics of the effective mass and the anomalous velocity in two-dimensional lattices

Y. Fang,* Federico Duque-Gomez,† and J. E. Sipe
*Department of Physics, University of Toronto, Toronto, Ontario, Canada M5S1A7*
(Received 22 July 2014; published 6 November 2014)

The semiclassical description of the dynamics of wave packets in periodic potentials and subject to an applied force relies on the concepts of effective mass and anomalous transport. This picture is valid if the force changes slowly in time and space, so that the particle described by the wave packet has time to respond according to the properties of the lattice. We analyze the dynamical corrections to this picture when a uniform force is suddenly applied, identifying separate corrections to the usual group and anomalous velocities. We find approximate semianalytical expressions for generalized "dynamical" group and anomalous velocities and the associated accelerations. We use a two-dimensional optical lattice with finite Berry curvature to illustrate the semianalytical approximation in a regime where the dynamical corrections are significant, suggesting the possibility of experiments to detect them; we compare the results with a full numerical solution, showing excellent agreement for weak forces.

DOI: 10.1103/PhysRevA.90.053407 PACS number(s): 37.10.Jk, 03.65.Sq, 03.65.Vf

## I. INTRODUCTION

The bands identified by the Bloch functions of a particle in a periodic potential have both spectral properties, such as their curvature, and topological properties, such as their Berry curvature. Both of these properties appear in the description of the dynamics of a wave packet. The role of the first is probably more well known. According to the *effective-mass theorem* [1], a particle moving in the presence of a periodic potential responds to an applied external force $\mathbf{F}$ with an *inverse effective-mass tensor*, according to

$$\frac{d^2}{dt^2}\langle \hat{r}^a \rangle = \left\langle \left[ \frac{1}{m_n^*(\mathbf{k})} \right]^{ab} \right\rangle F^b. \tag{1}$$

Here $\langle \hat{r}^a \rangle$ is the expectation value of the $a$th Cartesian component of the wave packet position, and repeated Cartesian components, labeled by $b$, are summed over. The expectation value on the right-hand side is the average over the wave packet of the *local inverse effective-mass tensor*, determined by the curvature of the band $n$ with which the wave packet is associated,

$$\left[ \frac{1}{m_n^*(\mathbf{k})} \right]^{ab} = \frac{1}{\hbar^2} \frac{\partial^2}{\partial k^a \partial k^b} [\hbar\omega_n(\mathbf{k})], \tag{2}$$

where $\hbar\omega_n(\mathbf{k})$ is the energy of the band as a function of wave vector $\mathbf{k}$. In the absence of time-reversal or space-inversion symmetry, this simple picture requires an extension due to the link between the dynamics of the particle and the topological properties of the bands [2–5]. Under the application of an external force, a wave packet additionally acquires an *anomalous velocity* [6–11], proportional to the curl of the applied force and the Berry curvature of the band with which the wave packet is associated, averaged over the wave packet.

The connection between the dynamics of wave packets and the spectral and topological properties of bands is thus central to the usual semiclassical description of transport in solid-state physics. However, in statements such as those above, it is important to be precise about what is meant by the "band with which the wave packet is associated." For a wave packet prepared strictly in one band, the validity of the effective-mass theorem and the anomalous transport relies on an adiabatic turning on of the force [12,13] since the wave packet cannot respond instantaneously according to the properties of the band structure. Upon such an application of the force, the wave packet acquires components of Bloch states of bands other than that which defined the initial wave packet; thus, the "associated band" has to be taken as that which mainly, but not exclusively, constitutes the wave packet.

In contrast to such a scenario, Pfirsch and Spenke showed that if a force is *suddenly* applied, a wave packet strictly in one band responds initially as if the lattice were not present; that is, the ratio of a component of the initial acceleration to the same component of the force is given by the inverse of the bare mass [14]. The response at later times is described by the usual effective mass only on average, as the expectation value of the acceleration oscillates about the usual semiclassical result [14–17]. Thus, there are instances when the usual semiclassical expressions fail. Nonetheless, for one-dimensional lattices it has been shown theoretically (see [18] and references therein) that for the sudden application of a force that is not too strong it is possible to define a *dynamical inverse effective mass* of a wave packet, defined as the ratio of the acceleration to the applied force. This quantity is a function of time, initially given by the inverse bare mass when the force is suddenly applied and oscillating at later times around the usual inverse effective mass as the wave packet moves through the Brillouin zone. Recently, this dynamical inverse effective mass has been experimentally observed in one-dimensional optical lattices [19].

This suggests that in lattices of higher dimensionality, where anomalous transport can arise, the breakdown of the effective-mass theorem should also be accompanied by corrections to the description of anomalous transport and that, for forces suddenly applied to a wave packet initially restricted to one band, it might be possible to identify a *dynamical anomalous velocity* of the wave packet. This would capture the fact that the anomalous velocity should initially vanish

*Present address: Department of Physics, University of California, Berkeley, California 94720-7300, USA.
†fduque@physics.utoronto.ca

 ©2014 American Physical Society

when the force is suddenly applied, since the wave packet cannot immediately respond to the lattice, and then it should eventually oscillate around the usual anomalous velocity that arises in the standard semiclassical description.

In this article we extend the description of the dynamics of wave packets subject to suddenly applied forces beyond the one-dimensional case [16,18] and find that this is, indeed, so. A semianalytical expression for the expectation value of the velocity is derived using modified Bloch states that decouple the bands in the presence of a uniform force neglecting Zener tunneling [20]; these states were introduced by Adams [7,12,21] and studied in more detail by Wannier [22]. We identify the usual *group velocity*, associated with the inverse effective-mass tensor, and the usual anomalous velocity. In addition, we find correction terms to first order in the force, which can be grouped in two terms with different mathematical structure; we interpret one of these terms as an oscillation of the group velocity and the other as an oscillation of the anomalous velocity. Thus, we can identify both a *dynamical group velocity* and a *dynamical anomalous velocity* of a wave packet, each of which differs from the usual semiclassical expression by oscillating terms. The time derivative of the sum of these is the expectation value of the acceleration of the wave packet. The time derivative of the dynamical group velocity is related to the applied force by the *dynamical inverse effective-mass tensor*, a generalization of the one-dimensional result mentioned above; this tensor is symmetric. The acceleration due to the oscillations in the dynamical anomalous velocity gives rise to an acceleration that is proportional to the force via an antisymmetric tensor; we refer to it as the *dynamical anomalous acceleration* of the wave packet.

The formalism is illustrated in a two-dimensional example with a tunable honeycomb optical lattice [23]; the lowest-energy band of this potential has finite local Berry curvature near the Dirac points. We study different trajectories in the Brillouin zone where the oscillations associated with the dynamical quantities mentioned above are significant. We test the validity of our semianalytic approach with a full numerical calculation and show that, for weak forces, our approach is valid over time scales of the order of a Bloch period, as it is for one dimensional lattices [18].

Our work is motivated by the recent observation of the dynamics of the effective mass with ultracold atoms in a one-dimensional optical lattice [19] and the availability of optical lattices of higher dimensionality [23–26]. Since optical lattices provide a clean and tunable periodic potential, they are an ideal platform for observing anomalous transport [27–30]. Furthermore, in this type of lattice the time scale associated with the dynamical oscillations of the effective mass and the anomalous velocity is much longer than in typical solid-state systems, where the period of the oscillations is expected to be of the order of femtoseconds [14,16,18] and the additional scattering due to impurities and phonons makes the detection of such oscillations more difficult. However, developments in time-resolved attosecond spectroscopy [31–34] suggest that the observation of electron dynamics in crystals in the subfemtosecond time scale is possible, opening the possibilities for studying the dynamics of the effective mass and the anomalous velocity presented here.

This article is organized as follows. In Sec. II we review the semiclassical expressions for the velocity and acceleration of a wave packet in a lattice of arbitrary dimensionality with an applied force. In Sec. III we show how these expressions are violated when the force is suddenly applied and how new dynamical quantities associated with the usual semiclassical expressions can be introduced. In Sec. IV we illustrate the semianalytical formulas with a two-dimensional optical lattice studied earlier by Tarruell *et al.* [23] and compare the results with a full numerical calculation. Finally, in Sec. V we present some conclusions.

## II. RESPONSE OF A WAVE PACKET IN A CRYSTAL TO A UNIFORM FORCE

In this section we present a careful derivation of the standard results of the semiclassical description of wave-packet dynamics in periodic potentials. After introducing our notation in Sec. II A, we present the modified Bloch states in Sec. II B, showing how wave packets constructed from them, which we call "modified Bloch state wave packets," provide the underpinning for the usual semiclassical expressions such as Eq. (1). The main results of this section are Eqs. (15) and (23), which describe the acceleration and the velocity of a wave packet in terms of the inverse effective-mass tensor, the group velocity, and the anomalous velocity.

### A. Crystal momentum representation

Consider a particle in a periodic potential, $V(\mathbf{r}+\mathbf{R}) = V(\mathbf{r})$, where $\mathbf{R}$ is a lattice vector. In the presence of an external uniform force $\mathbf{F}(t)$, the Hamiltonian for the system can be written as

$$\hat{H}(t) = \hat{H}_o - \mathbf{F}(t)\cdot\hat{\mathbf{r}}, \tag{3}$$

where

$$\hat{H}_o \equiv \frac{\hat{\mathbf{p}}^2}{2m} + V(\hat{\mathbf{r}})$$

is the unperturbed Hamiltonian in terms of the momentum operator $\hat{\mathbf{p}}$ and the bare mass $m$. The Bloch states that diagonalize $\hat{H}_o$,

$$\hat{H}_o\,|\psi_{n\mathbf{k}}\rangle = \hbar\omega_n(\mathbf{k})\,|\psi_{n\mathbf{k}}\rangle,$$

have the form

$$\psi_{n\mathbf{k}}(\mathbf{r}) \equiv \langle\mathbf{r}|\psi_{n\mathbf{k}}\rangle = \frac{1}{\sqrt{(2\pi)^{\mathcal{D}}}}u_{n\mathbf{k}}(\mathbf{r})e^{i\mathbf{k}\cdot\mathbf{r}} \tag{4}$$

in real space and are labeled by a band index $n$ and a wave vector $\mathbf{k}$. In Eq. (4), $\mathcal{D}$ denotes the dimensionality of the lattice (for example, $\mathcal{D}=2$ for a two-dimensional lattice), and the function $u_{n\mathbf{k}}(\mathbf{r}) \equiv \langle\mathbf{r}|u_{n\mathbf{k}}\rangle$ has the periodicity of the lattice, $u_{n\mathbf{k}}(\mathbf{r}+\mathbf{R}) = u_{n\mathbf{k}}(\mathbf{r})$. In the crystal momentum representation [35], the state of the particle is written as a wave packet of Bloch states

$$|\Psi(t)\rangle = \sum_n \int_{\mathrm{BZ}} d\mathbf{k}\, c_n(\mathbf{k},t)\,|\psi_{n\mathbf{k}}\rangle,$$

where BZ denotes integration over the (first) Brillouin zone, and the $a$th Cartesian component of the position operator [35]

$$\begin{aligned}\langle\psi_{n_1\mathbf{k}_1}|\hat{r}^a|\psi_{n_2\mathbf{k}_2}\rangle &\equiv \int d\mathbf{r}\,\psi^*_{n_1\mathbf{k}_1}(\mathbf{r})r^a\psi_{n_2\mathbf{k}_2}(\mathbf{r})\\ &= \delta_{n_1n_2}\left(-i\frac{\partial}{\partial k_2^a}\delta(\mathbf{k}_1-\mathbf{k}_2)\right)\\ &\quad+\delta(\mathbf{k}_1-\mathbf{k}_2)\xi^a_{n_1n_2}(\mathbf{k}_1)\end{aligned}\tag{5}$$

is expressed in terms of the matrix elements [36]

$$\begin{aligned}\xi^a_{n_1n_2}(\mathbf{k}) &\equiv \langle u_{n_1\mathbf{k}}|i\frac{\partial}{\partial k^a}|u_{n_2\mathbf{k}}\rangle\\ &\equiv \int_{V_{\rm cell}}\frac{d\mathbf{r}}{V_{\rm cell}}\,u^*_{n_1\mathbf{k}}(\mathbf{r})i\frac{\partial}{\partial k^a}u_{n_2\mathbf{k}}(\mathbf{r}).\end{aligned}\tag{6}$$

Note that the integration in Eq. (5) and in any matrix element of the form $\langle\psi_{n_1\mathbf{k}_1}|\cdot|\psi_{n_2\mathbf{k}_2}\rangle$ is over *all space*; on the other hand, the integration in Eq. (6) and in any matrix element of the form $\langle u_{n_1\mathbf{k}}|\cdot|u_{n_2\mathbf{k}}\rangle$ is over *one unit cell*, with volume $V_{\rm cell}$.

Similarly, for the momentum operator we have

$$\begin{aligned}\left\langle\psi_{n_1\mathbf{k}_1}|\hat{p}^a|\psi_{n_2\mathbf{k}_2}\right\rangle &\equiv \int d\mathbf{r}\,\psi^*_{n_1\mathbf{k}_1}(\mathbf{r})\frac{\hbar}{i}\frac{\partial}{\partial r^a}\psi_{n_2\mathbf{k}_2}(\mathbf{r})\\ &= \delta(\mathbf{k}_1-\mathbf{k}_2)p^a_{n_1n_2}(\mathbf{k}_1),\end{aligned}$$

where [35]

$$p^a_{n_1n_2}(\mathbf{k}) \equiv \delta_{n_1n_2}\hbar k^a + \langle u_{n_1\mathbf{k}}|\hat{p}^a|u_{n_2\mathbf{k}}\rangle.$$

For nondegenerate bands, the off-diagonal elements of Eq. (6) are related to the momentum matrix elements by [36]

$$\xi^a_{n_1n_2}(\mathbf{k}) = \frac{1}{im}\frac{p^a_{n_1n_2}(\mathbf{k})}{\omega_{n_1n_2}(\mathbf{k})}\ [\text{for}\ \omega_{n_1}(\mathbf{k})\neq\omega_{n_2}(\mathbf{k})],$$

where $\omega_{n_1n_2}(\mathbf{k})\equiv\omega_{n_1}(\mathbf{k})-\omega_{n_2}(\mathbf{k})$. The diagonal element $\boldsymbol{\xi}_{nn}(\mathbf{k})$ is known as the *Berry connection*. Despite being "gauge dependent" in that it depends on how the phases of the Bloch states are set throughout the Brillouin zone, the Berry connection has dynamical consequences through the *Berry curvature* [6–8,10], which is gauge independent. The local Berry curvature $\boldsymbol{\Omega}_n(\mathbf{k})$ has components given by

$$\Omega^l_n(\mathbf{k}) \equiv \epsilon^{lab}\frac{\partial}{\partial k^a}\xi^b_{nn}(\mathbf{k}),\tag{7}$$

where $\epsilon^{lab}$ is the antisymmetric Levi-Civita symbol and repeated Cartesian components are summed over.

### B. Modified Bloch states, the effective-mass theorem, and anomalous transport

For a wave packet subjected to a force $\mathbf{F}(t)$ [see Eq. (3)] and described by a ket $|\Psi(t)\rangle$, the expectation value of the acceleration follows from Ehrenfest's theorem,

$$\begin{aligned}\langle\hat{\mathbf{a}}(t)\rangle &\equiv \frac{d^2}{dt^2}\langle\Psi(t)|\hat{\mathbf{r}}|\Psi(t)\rangle\\ &= \frac{\mathbf{F}(t)}{m}+\frac{1}{i\hbar m}\langle\Psi(t)|[\hat{\mathbf{p}},\hat{H}_o]|\Psi(t)\rangle.\end{aligned}\tag{8}$$

Suppose now we consider a force that turns on at $t=0$, $\mathbf{F}(t)=\mathbf{0}$ for $t<0$ and $\mathbf{F}(t)=\mathbf{F}$ for $t\geqslant 0$. If, initially, the wave packet is formed only by Bloch states from a single band, say, band $N$,

$$|\Psi(0)\rangle = |\bar{\psi}_N\rangle \equiv \int_{\rm BZ} d\mathbf{k}\,f_N(\mathbf{k})|\psi_{N\mathbf{k}}\rangle,\tag{9}$$

at $t=0$ the commutator in Eq. (8) vanishes, and we have $\langle\hat{\mathbf{a}}(0^+)\rangle = \mathbf{F}/m$. That is, the wave packet responds initially with the inverse *bare* mass of the particle and not the inverse effective-mass tensor. This is an old result [14–17]: a wave packet formed by Bloch states from a single band does not respond to the periodic potential of the lattice when the force is applied, and at very early times the particle generally responds to an applied force as if it were free. At later times the wave packet cannot remain in only one band, as the force inevitably couples the Bloch states of different bands, and it is through this coupling that the lattice makes itself felt. However, we can still define a wave packet that remains *mainly* in one band and responds essentially with the properties of that band; the amplitudes of such a wave packet in neighboring bands are due to the interband mixing induced by the force.

In a treatment that was later shown to be correct if Zener tunnelling is neglected [20], Wannier found that for a constant and uniform force, $\mathbf{F}(t)=\mathbf{F}$, the interband mixing can be captured by *modified Bloch states* $|\phi_{n\mathbf{k}}\rangle$ that are related to the original Bloch states $|\psi_{n\mathbf{k}}\rangle$ by a unitary transformation [22],

$$|\phi_{n\mathbf{k}}\rangle \equiv \sum_{n'}|\psi_{n'\mathbf{k}}\rangle\,U_{n'n}(\mathbf{k}).\tag{10}$$

The unitary transformation $U_{n'n}(\mathbf{k})$ can be constructed to different orders in the force [18,22]; in the first-order approximation and assuming no degeneracies [37], these modified Bloch states take the form

$$|\phi_{n\mathbf{k}}\rangle \approx |\psi_{n\mathbf{k}}\rangle + \sum_{n'}|\psi_{n'\mathbf{k}}\rangle\,\Delta_{n'n}(\mathbf{k}),$$

where $\Delta(\mathbf{k})$ is an off-diagonal matrix with elements [18,21]

$$\Delta_{n_1n_2}(\mathbf{k}) \equiv \frac{F^b\xi^b_{n_1n_2}(\mathbf{k})}{\hbar\omega_{n_1n_2}(\mathbf{k})}(1-\delta_{n_1n_2}).$$

As a result of this construction, a wave packet formed only by modified Bloch states associated with band $N$,

$$|\bar{\phi}_N(0)\rangle = \int_{\rm BZ} d\mathbf{k}\,\bar{b}_N(\mathbf{k})\,|\phi_{N\mathbf{k}}\rangle\,,$$

evolves in time moving through the Brillouin zone without mixing with other modified Bloch states from neighboring bands. To first order in the force, we find [18,22]

$$|\bar{\phi}_N(t)\rangle = \int_{\rm BZ} d\mathbf{k}\,\bar{b}_N(\boldsymbol{\kappa})e^{-i\gamma_N(\boldsymbol{\kappa},t)}|\phi_{N\mathbf{k}}\rangle,\tag{11}$$

where $\boldsymbol{\kappa}\equiv\mathbf{k}-\mathbf{F}t/\hbar$ and

$$\gamma_n(\mathbf{k},t)\equiv\int_0^t\left[\omega_n\left(\mathbf{k}+\frac{1}{\hbar}\mathbf{F}t'\right)-\frac{1}{\hbar}\mathbf{F}\cdot\boldsymbol{\xi}_{nn}\left(\mathbf{k}+\frac{1}{\hbar}\mathbf{F}t'\right)\right]dt'.$$

We refer to the wave packet $|\bar{\phi}_N(t)\rangle$ as a MBS wave packet, where MBS stands for modified Bloch state. This type of wave packet satisfies the effective-mass theorem *at all times*. This

can be shown by using the matrix elements [18]

$$\mathfrak{F}^a_{n_1n_2}(\mathbf{k}) \equiv i \sum_{n_1',n_2'} U^\dagger_{n_1n_1'}(\mathbf{k}) p^a_{n_1'n_2'}(\mathbf{k}) \omega_{n_1'n_2'}(\mathbf{k})\, U_{n_2'n_2}(\mathbf{k})$$

to rewrite Eq. (8) for $|\bar{\phi}_N(t)\rangle$ as

$$\frac{d^2}{dt^2}\langle\bar{\phi}_N(t)|\hat{r}^a|\bar{\phi}_N(t)\rangle = \frac{F^a}{m} + \int_{\mathrm{BZ}} d\mathbf{k}\, |\bar{b}_N(\boldsymbol{\kappa})|^2 \mathfrak{F}^a_{NN}(\mathbf{k}). \quad (12)$$

To first order in the force, we can write

$$\mathfrak{F}^a_{NN}(\mathbf{k}) \approx \frac{1}{m}\sum_{n\neq N} \frac{p^a_{Nn}(\mathbf{k})p^b_{nN}(\mathbf{k}) + p^b_{Nn}(\mathbf{k})p^a_{nN}(\mathbf{k})}{\hbar\omega_{Nn}(\mathbf{k})} F^b, \quad (13)$$

and the sum rule for the local inverse effective-mass tensor [36],

$$m\left[\frac{1}{m^*_N(\mathbf{k})}\right]^{ab} - \delta^{ab} = \frac{1}{m}\sum_{n\neq N} \frac{p^a_{Nn}(\mathbf{k})p^b_{nN}(\mathbf{k}) + p^b_{Nn}(\mathbf{k})p^a_{nN}(\mathbf{k})}{\hbar\omega_{Nn}(\mathbf{k})}, \quad (14)$$

reduces Eq. (12) to

$$\frac{d^2}{dt^2}\langle\bar{\phi}_N(t)|\hat{r}^a|\bar{\phi}_N(t)\rangle = \int_{\mathrm{BZ}} d\mathbf{k}\, |\bar{b}_N(\boldsymbol{\kappa})|^2 \left[\frac{1}{m^*_N(\mathbf{k})}\right]^{ab} F^b, \quad (15)$$

in accordance with the effective-mass theorem, Eq. (1). Note that, compared with Eq. (2), the sum rule in Eq. (14) reveals the truly multiband nature of the local inverse effective-mass tensor [38], which is reflected in the use of modified Bloch states to construct a wave packet that responds with the effective mass *at all times*.

We can follow the same strategy for the expectation value of the velocity. We find

$$\langle\hat{\mathbf{v}}(t)\rangle \equiv \frac{d}{dt}\langle\Psi(t)|\hat{\mathbf{r}}|\Psi(t)\rangle = \frac{1}{m}\langle\Psi(t)|\hat{\mathbf{p}}|\Psi(t)\rangle \quad (16)$$

[see Eq. (8)]. In the particular case of a MBS wave packet, $|\Psi(t)\rangle = |\bar{\phi}_N(t)\rangle$, Eq. (16) becomes

$$\frac{d}{dt}\langle\bar{\phi}_N(t)|\hat{r}^a|\bar{\phi}_N(t)\rangle = \int_{\mathrm{BZ}} d\mathbf{k}\, |\bar{b}_N(\boldsymbol{\kappa})|^2 \frac{1}{m}\mathfrak{P}^a_{NN}(\mathbf{k}), \quad (17)$$

where $\mathfrak{P}^a_{n_1n_2}(\mathbf{k})$ are the transformed momentum matrix elements,

$$\mathfrak{P}^a_{n_1n_2}(\mathbf{k}) \equiv \sum_{n_1',n_2'} U^\dagger_{n_1n_1'}(\mathbf{k}) p^a_{n_1'n_2'}(\mathbf{k}) U_{n_2'n_2}(\mathbf{k}).$$

Analogous to Eq. (13), the diagonal elements $\mathfrak{P}^a_{NN}(\mathbf{k})$ have a simple form to first order in the force,

$$\frac{1}{m}\mathfrak{P}^a_{NN}(\mathbf{k}) \approx v^{\mathrm{g},a}_N(\mathbf{k}) + \frac{1}{\hbar}\mathfrak{J}^{ab}_{NN}(\mathbf{k})F^b. \quad (18)$$

The first term in this expression corresponds to the *local group velocity* [36],

$$v^{\mathrm{g},a}_N(\mathbf{k}) \equiv \frac{p^a_{NN}(\mathbf{k})}{m} = \frac{1}{\hbar}\frac{\partial}{\partial k^a}[\hbar\omega_N(\mathbf{k})], \quad (19)$$

given by the gradient of the band energy; this term is directly related to the local inverse effective-mass tensor since

$$\begin{aligned}\frac{d}{dt}\int_{\mathrm{BZ}} d\mathbf{k}\, |\bar{b}_N(\boldsymbol{\kappa})|^2\, v^{\mathrm{g},a}_N(\mathbf{k}) &= -\int_{\mathrm{BZ}} d\mathbf{k}\left(\frac{\partial}{\partial k^b}|\bar{b}_N(\boldsymbol{\kappa})|^2\right)\frac{1}{\hbar^2}\frac{\partial}{\partial k^a}(\hbar\omega_N(\mathbf{k}))F^b \\ &= \int_{\mathrm{BZ}} d\mathbf{k}\, |\bar{b}_N(\boldsymbol{\kappa})|^2 \left[\frac{1}{m^*_n(\mathbf{k})}\right]^{ab} F^b. \end{aligned} \quad (20)$$

The contribution from the first term on the right-hand side of Eq. (18) to Eq. (17) is not surprising; as a wave packet simply moves through the Brillouin zone at a pace proportional to the force, it acquires the group velocity [see Eq. (19)] associated with the band energy. The second term on the right-hand side of Eq. (18), on the other hand, has a completely different structure given by the antisymmetric tensor

$$\mathfrak{J}^{ab}_{NN}(\mathbf{k}) \equiv \sum_{n\neq N} 2\,\mathrm{Im}\big[\xi^a_{Nn}(\mathbf{k})\xi^b_{nN}(\mathbf{k})\big]. \quad (21)$$

As a result of the sum rule [36]

$$\epsilon^{alb}\Omega^l_N(\mathbf{k}) = \sum_{n\neq N} 2\,\mathrm{Im}\big[\xi^a_{Nn}(\mathbf{k})\xi^b_{nN}(\mathbf{k})\big],$$

the second term on the right-hand side of Eq. (18) becomes the *local anomalous velocity* [7],

$$v^{\mathrm{an},a}_N(\mathbf{k}) \equiv \frac{1}{\hbar}\epsilon^{alb}\Omega^l_N(\mathbf{k})F^b, \quad (22)$$

a first-order correction to the velocity associated with the local Berry curvature, Eq. (7). Thus, we can rewrite Eq. (17) as

$$\frac{d}{dt}\langle\bar{\phi}_N(t)|\hat{r}^a|\bar{\phi}_N(t)\rangle = \int_{\mathrm{BZ}} d\mathbf{k}\, |\bar{b}_N(\boldsymbol{\kappa})|^2\big[v^{\mathrm{g},a}_N(\mathbf{k}) + v^{\mathrm{an},a}_N(\mathbf{k})\big], \quad (23)$$

including both the group velocity and the anomalous velocity of the wave packet [9]. These velocities are periodic in time as the wave packet traverses the Brillouin zone and returns to its starting point in reciprocal space; the period of this motion in reciprocal space is the Bloch period $\tau_B$ [39]. The anomalous transport correction to the usual effective-mass behavior is only important for potentials that break space-inversion symmetry or time-reversal symmetry, where the local Berry curvature is different from zero [40]. Note that if we calculate the time derivative of Eq. (23) and keep terms linear in the force, we get the same result as Eq. (15) since the time derivative of the anomalous velocity does not contribute to first order in the force, while the time derivative of the group velocity contributes the acceleration described by the usual inverse effective-mass tensor [see Eq. (20)].

## III. DYNAMICS OF THE EFFECTIVE MASS AND THE ANOMALOUS VELOCITY

We can employ the modified Bloch states to describe the motion of a wave packet that originally consists of a superposition of the usual Bloch states from band $N$, as in Eq. (9), when a force is applied. Were the force increased *adiabatically* from zero to $\mathbf{F}$, the wave packet would acquire

the particular composition required to move according to Eqs. (15) and (23) [12,13]. But if the force is applied instantaneously, for $t > 0$, we can seek an expansion of the ket $|\Psi(t)\rangle$ as a superposition of MBS wave packets [see Eq. (11)], with coefficients chosen so that at $t = 0$ the state yields Eq. (9). To linear order in the force, which is the order to which we have constructed $|\phi_{n\mathbf{k}}\rangle$, this can be easily done; to zeroth order $|\Psi(t)\rangle$ will just be the appropriate $|\bar{\phi}_N(t)\rangle$, and to first order there will be contributions from other $|\bar{\phi}_n(t)\rangle$ with $n \neq N$ [18]. In this scenario we will see that there is a transition from the bare-mass response to the semiclassical dynamics described by the local inverse effective-mass tensor, Eq. (2), and the local anomalous velocity, Eq. (22); the transition is characterized by oscillations of the acceleration and the velocity around the values predicted by Eqs. (15) and (23). We now establish those dynamics.

Following [18], the ket for $t \geqslant 0$ is

$$|\Psi(t)\rangle = \sum_n \int_{\mathrm{BZ}} d\mathbf{k}\, b_n(\mathbf{k},t)\, |\phi_{n\mathbf{k}}\rangle\,, \tag{24}$$

where to first order in the force

$$b_N(\mathbf{k},t) = f_N(\boldsymbol{\kappa}) e^{-i\gamma_N(\boldsymbol{\kappa},t)}, \tag{25}$$

$$b_n(\mathbf{k},t) = -f_N(\boldsymbol{\kappa})\Delta_{nN}(\boldsymbol{\kappa}) e^{-i\gamma_n(\boldsymbol{\kappa},t)}. \tag{26}$$

The expectation value of the velocity,

$$\langle \hat{v}^a(t)\rangle = \frac{1}{m}\sum_{n_1,n_2}\int_{\mathrm{BZ}} d\mathbf{k}\, b^*_{n_1}(\mathbf{k},t) b_{n_2}(\mathbf{k},t)\mathfrak{P}^a_{n_1n_2}(\mathbf{k}),$$

can be split into three terms,

$$\langle \hat{v}^a(t)\rangle \approx \int_{\mathrm{BZ}} d\mathbf{k}\, |f_N(\boldsymbol{\kappa})|^2 \big[v_N^{\mathrm{g},a}(\mathbf{k}) + v_N^{\mathrm{an},a}(\mathbf{k}) + \mathcal{V}_N^a(\mathbf{k},t)\big]. \tag{27}$$

This approximate expression for the wave-packet velocity is expected to be accurate for forces such that $\Delta_{nN}(\mathbf{k})$ is small [18,21,22]; roughly, this requirement means that the energy drop over one unit cell associated with the force should be small compared with the energy gap between the starting band $N$ and its closest neighboring band. The first two contributions in Eq. (27) involve the usual group velocity from Eq. (19) and the anomalous velocity from Eq. (22). In the additional term, $\mathcal{V}_N^a(\mathbf{k},t)$ can be written as

$$\mathcal{V}_N^a(\mathbf{k},t) = -\frac{1}{\hbar}\mathcal{J}_N^{ab}(\mathbf{k},t)F^b,$$

where the tensor

$$\mathcal{J}_N^{ab}(\mathbf{k},t) \equiv \sum_{n\neq N}\frac{\omega_{nN}(\mathbf{k})}{\omega_{nN}(\boldsymbol{\kappa})} 2\,\mathrm{Im}\big[\xi^a_{Nn}(\mathbf{k})\xi^b_{nN}(\boldsymbol{\kappa}) e^{-i\gamma_{nN}(\boldsymbol{\kappa},t)}\big] \tag{28}$$

is a time-dependent generalization of Eq. (21) with $\gamma_{n_1n_2}(\mathbf{k},t) \equiv \gamma_{n_1}(\mathbf{k},t) - \gamma_{n_2}(\mathbf{k},t)$. We will see that $\mathcal{V}_N^a(\mathbf{k},t)$ describes oscillations of $\langle \hat{v}^a(t)\rangle$ about the result given by Eq. (23). At $t = 0$, $\mathcal{J}_N^{ab}(\mathbf{k},t)$ reduces to the antisymmetric tensor $\mathfrak{J}_{NN}^{ab}(\mathbf{k})$, but for $t > 0$, it does not have definite symmetry. Nevertheless, we can still decompose $\mathcal{J}_N^{ab}(\mathbf{k},t)$ uniquely into symmetric and antisymmetric parts,

$$\mathcal{J}_N^{ab}(\mathbf{k},t) = \bar{\mathcal{J}}_N^{ab}(\mathbf{k},t) + \check{\mathcal{J}}_N^{ab}(\mathbf{k},t), \tag{29}$$

where

$$\bar{\mathcal{J}}_N^{ab}(\mathbf{k},t) \equiv \tfrac{1}{2}\big[\mathcal{J}_N^{ab}(\mathbf{k},t) + \mathcal{J}_N^{ba}(\mathbf{k},t)\big], \tag{30}$$

$$\check{\mathcal{J}}_N^{ab}(\mathbf{k},t) \equiv \tfrac{1}{2}\big[\mathcal{J}_N^{ab}(\mathbf{k},t) - \mathcal{J}_N^{ba}(\mathbf{k},t)\big]. \tag{31}$$

The antisymmetric part, Eq. (31), can also be expressed in terms of the axial vector $\boldsymbol{\Lambda}_N(\mathbf{k},t)$ with components

$$\Lambda_N^l(\mathbf{k},t) \equiv -\tfrac{1}{2}\epsilon^{lab}\check{\mathcal{J}}_N^{ab}(\mathbf{k},t), \tag{32}$$

so that

$$\check{\mathcal{J}}_N^{ab}(\mathbf{k},t) = \epsilon^{alb}\Lambda_N^l(\mathbf{k},t).$$

Defining

$$X^{\pm,ab}_{Nn}(\mathbf{k},t) \equiv \xi^a_{Nn}(\mathbf{k})\xi^b_{nN}(\boldsymbol{\kappa}) e^{-i\gamma_{nN}(\boldsymbol{\kappa},t)} \pm \xi^a_{Nn}(\boldsymbol{\kappa}) e^{-i\gamma_{Nn}(\boldsymbol{\kappa},t)}\xi^b_{nN}(\mathbf{k}),$$

Eqs. (30) and (32) become

$$\bar{\mathcal{J}}_N^{ab}(\mathbf{k},t) = \sum_{n\neq N}\mathrm{Im}\big[X^{-,ab}_{Nn}(\mathbf{k},t)\big]\frac{\omega_{nN}(\mathbf{k})}{\omega_{nN}(\boldsymbol{\kappa})} \tag{33}$$

and

$$\Lambda_N^l(\mathbf{k},t) = -\frac{1}{2}\epsilon^{lab}\sum_{n\neq N}\mathrm{Im}\big[X^{+,ab}_{Nn}(\mathbf{k},t)\big]\frac{\omega_{nN}(\mathbf{k})}{\omega_{nN}(\boldsymbol{\kappa})}, \tag{34}$$

respectively.

With this formal decomposition in hand, we link some of the dynamical oscillations described by $\mathcal{V}_N^a(\mathbf{k},t)$ with the group velocity and some with the anomalous velocity by rewriting Eq. (27) for $\langle \hat{v}^a(t)\rangle$ as

$$\langle \hat{v}^a(t)\rangle \approx V^{\mathrm{g},a}(t) + V^{\mathrm{an},a}(t), \tag{35}$$

where we identify the *dynamical group velocity* $\mathbf{V}^{\mathrm{g}}(t)$ of the wave packet, with components

$$V^{\mathrm{g},a}(t) \equiv \int_{\mathrm{BZ}} d\mathbf{k}\, |f_N(\boldsymbol{\kappa})|^2\left(v_N^{\mathrm{g},a}(\mathbf{k}) - \frac{1}{\hbar}\bar{\mathcal{J}}_N^{ab}(\mathbf{k},t)F^b\right), \tag{36}$$

and the *dynamical anomalous velocity* $\mathbf{V}^{\mathrm{an}}(t)$ of the wave packet, with components

$$V^{\mathrm{an},a}(t) \equiv \int_{\mathrm{BZ}} d\mathbf{k}\, |f_N(\boldsymbol{\kappa})|^2\left(v_N^{\mathrm{an},a}(\mathbf{k}) - \frac{1}{\hbar}\check{\mathcal{J}}_N^{ab}(\mathbf{k},t)F^b\right). \tag{37}$$

The leading terms in parentheses in the integrands in Eqs. (36) and (37) are the contributions that would be expected from a MBS wave packet associated with band $N$ [see Eq. (23)]; the other terms in parentheses give oscillatory corrections. Note that Eq. (37) can be written as

$$V^{\mathrm{an},a}(t) = \frac{1}{\hbar}\epsilon^{alb}\Omega_N^l(t)F^b, \tag{38}$$

where

$$\boldsymbol{\Omega}_N(t) \equiv \int_{\mathrm{BZ}} d\mathbf{k}\, |f_N(\boldsymbol{\kappa})|^2[\boldsymbol{\Omega}_N(\mathbf{k}) - \boldsymbol{\Lambda}_N(\mathbf{k},t)]$$

can be interpreted as the *dynamical Berry curvature* "seen" by the wave packet as it moves through the Brillouin zone.

The identification of the term involving $\bar{\mathcal{J}}_N^{ab}(\mathbf{k},t)$ with the group velocity of the wave packet is justified by the fact that the time derivative of $\mathbf{V}^{\mathrm{g}}(t)$,

$$\mathbf{A}^{\mathrm{g}}(t) \equiv \frac{d}{dt}\mathbf{V}^{\mathrm{g}}(t),$$

is found to have components

$$A^{\mathrm{g},a}(t) = \left[\frac{1}{M^*(t)}\right]^{ab} F^b,$$

where we have introduced a *dynamical inverse effective-mass tensor*,

$$\left[\frac{1}{M^*(t)}\right]^{ab} \equiv \int_{\mathrm{BZ}} d\mathbf{k}\,|f_N(\boldsymbol{\kappa})|^2 \left(\left[\frac{1}{m_N^*(\mathbf{k})}\right]^{ab} - \frac{1}{m}\bar{\mathcal{K}}_N^{ab}(\mathbf{k},t)\right), \tag{39}$$

and where the tensor

$$\bar{\mathcal{K}}_N^{ab}(\mathbf{k},t) \equiv -\frac{m}{\hbar}\sum_{n\neq N} \mathrm{Re}\left[X_{Nn}^{+,ab}(\mathbf{k},t)\right]\frac{[\omega_{nN}(\mathbf{k})]^2}{\omega_{nN}(\boldsymbol{\kappa})} \tag{40}$$

is *symmetric* with respect to its Cartesian components in the same way as the local inverse effective-mass tensor [Eq. (2)], leading to a dynamical inverse effective-mass tensor that is symmetric. The first contribution in parentheses in the integrand of Eq. (39) gives the result that would be expected for a MBS wave packet [see Eq. (15)]; the term involving $\bar{\mathcal{K}}_N^{ab}(\mathbf{k},t)$ describes oscillatory corrections. The time derivative of the expectation value of the velocity written in the form of Eq. (35),

$$\langle\hat{\mathbf{a}}(t)\rangle = \frac{d}{dt}\langle\hat{\mathbf{v}}(t)\rangle = \mathbf{A}^{\mathrm{g}}(t) + \mathbf{A}^{\mathrm{an}}(t), \tag{41}$$

includes a *dynamical anomalous acceleration* $\mathbf{A}^{\mathrm{an}}(t)$, which is the time derivative of $\mathbf{V}^{\mathrm{an}}(t)$. This dynamical anomalous acceleration is perpendicular to the force, and it has components

$$A^{\mathrm{an},a}(t) = \int_{\mathrm{BZ}} d\mathbf{k}\,|f_N(\boldsymbol{\kappa})|^2\left(-\frac{1}{m}\check{\mathcal{K}}_N^{ab}(\mathbf{k},t)\right)F^b,$$

given by the *antisymmetric* tensor

$$\check{\mathcal{K}}_N^{ab}(\mathbf{k},t) \equiv \epsilon^{alb}\,\Xi_N^l(\mathbf{k},t), \tag{42}$$

where

$$\Xi_N^l(\mathbf{k},t) \equiv \frac{m}{2\hbar}\epsilon^{lab}\sum_{n\neq N}\mathrm{Re}\left[X_{Nn}^{-,ab}(\mathbf{k},t)\right]\frac{[\omega_{nN}(\mathbf{k})]^2}{\omega_{nN}(\boldsymbol{\kappa})}$$

are the components of an axial vector. Unlike the dynamical inverse effective-mass tensor and the acceleration it describes, to first order in the force the dynamical anomalous acceleration contains only oscillatory terms [see the discussion after Eq. (23)]. Note that the acceleration in Eq. (41) can also be derived directly from Ehrenfest's theorem using Eq. (8) with the wave packet given by Eq. (24).

At the initial time, Eqs. (33) and (34) reduce to

$$\bar{\mathcal{J}}_N^{ab}(\mathbf{k},0) = 0, \quad \Lambda_N^l(\mathbf{k},0) = \Omega_N^l(\mathbf{k}),$$

so

$$V^{\mathrm{g},a}(0) = \int_{\mathrm{BZ}} d\mathbf{k}\,|f_N(\mathbf{k})|^2\,v_N^{\mathrm{g},a}(\mathbf{k}), \quad V^{\mathrm{an},a}(0) = 0, \tag{43}$$

consistent with the initial behavior found using Ehrenfest's theorem for the initial state [Eq. (9)]; initially, the Berry curvature "seen" by the wave packet vanishes, and there is no anomalous velocity. For $t > 0$, the wave packet's velocity acquires dynamical oscillations around the usual group velocity, in a way similar to that for the earlier results found for one-dimensional lattices [18]. Since at the initial time

$$\bar{\mathcal{K}}_N^{ab}(\mathbf{k},0) = m\left[\frac{1}{m_N^*(\mathbf{k})}\right]^{ab} - \delta^{ab}, \quad \check{\mathcal{K}}_N^{ab}(\mathbf{k},0) = 0$$

[see Eqs. (14), (40), and (42)], the dynamical inverse effective-mass tensor is initially given by the inverse bare mass,

$$\left[\frac{1}{M^*(0)}\right]^{ab} = \frac{\delta^{ab}}{m}, \quad A^{\mathrm{an},a}(0) = 0. \tag{44}$$

Hence, the particle initially responds with the bare mass [14,15,18]; afterwards, the dynamical inverse effective-mass tensor acquires oscillations about the usual inverse effective-mass tensor. In addition, the anomalous transport described by $\mathbf{V}^{\mathrm{an}}(t)$ has its own dynamics; rather than just the Berry curvature, it is governed by the dynamical Berry curvature $\Omega_N^l(t)$, which contains its own oscillatory terms.

## IV. EXAMPLE

We now apply the semianalytical expressions for the dynamics of wave packets to a two-dimensional optical lattice. We begin with the band structure and local Berry curvature of the lattice we consider (Sec. IV A). A wave packet built in the first band with a Gaussian envelope function is then set along different trajectories in the Brillouin zone; its dynamics are calculated through the semianalytical approach (Sec. IV B). Finally, this result is compared with a full numerical solution (Sec. IV C).

### A. Two-dimensional optical lattice

We consider the optical lattice described by Tarruell *et al.* [23], created by the interference of three retroreflected laser beams, which leads to a potential

$$\begin{aligned} V(x,y) &= \frac{-V_{\bar{X}}}{2}\cos[K(x+y)+\theta] - \frac{V_X}{2}\cos[K(x+y)] \\ &\quad - \frac{V_Y}{2}\cos[K(x-y)] - \sqrt{V_X V_Y}[\cos(Kx)+\cos(Ky)] \\ &\quad - \frac{1}{2}(V_{\bar{X}} + V_X + V_Y), \end{aligned} \tag{45}$$

where $V_X$, $V_Y$, and $V_{\bar{X}}$ are proportional to the intensities of each of the laser beams and the phase $\theta$ is controlled by a small detuning between lasers associated with $V_X$ and $V_{\bar{X}}$ [41]. We use values of $V_X = 0.25E_R$, $V_Y = 1.0E_R$, and $V_{\bar{X}} = 3.5E_R$, where

$$E_R \equiv \frac{\hbar^2 K^2}{2m}$$

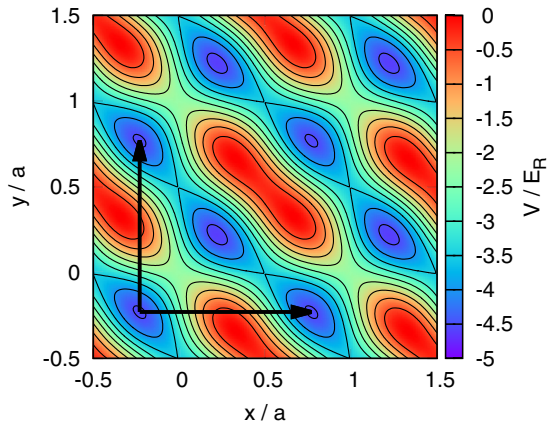


FIG. 1. (Color online) Honeycomb lattice given by Eq. (45) for $V_X = 0.25E_R$, $V_Y = 1.0E_R$, $V_{\bar{X}} = 3.5E_R$, and $\theta = 1.02\pi$. The $x$ and $y$ axes give the position in units of the lattice constant. The color plot shows the value of the potential in units of the recoil energy $E_R$. Two lattice vectors are also shown with black arrows.

is a recoil energy. In addition to $E_R$, another important physical quantity is the recoil velocity

$$v_R \equiv \frac{\hbar K}{m},$$

which will be used in the velocity plots discussed in Secs. IV B and IV C. The lattice vectors in real space are in the $\hat{\mathbf{x}}$ and $\hat{\mathbf{y}}$ directions and have magnitude $a = \lambda/\sqrt{2}$, where $\lambda$ is the wavelength of all three lasers; for the experiments described by Tarruell *et al.* [23], $\lambda = 1064$ nm. The reciprocal lattice vectors are in the $\hat{\mathbf{x}}$ and $\hat{\mathbf{y}}$ directions with magnitude

$$K = \frac{2\pi}{a},$$

which is also the linear dimension of the Brillouin zone. The potential resembles a squeezed honeycomb lattice and is shown in Fig. 1; we also show the energy spectrum for the two lowest bands of this potential in Fig. 2. In the next section we will study the motion of a wave packet in the lowest band of this potential; Figs. 3 and 4 illustrate the Berry curvature and energy dispersion of this band, which determine the wave-packet dynamics in the usual semiclassical picture.

When $\theta$ is set to $\pi$, the lattice satisfies space-inversion symmetry, and the two lowest-energy bands intersect each other at two Dirac points. In this case, the local Berry curvature is zero everywhere except at the two Dirac points, where it is singular [42]. However, tuning $\theta$ to values slightly different from $\pi$ breaks space-inversion symmetry, opens up a band gap (see Fig. 2), and results in a more well-behaved local Berry curvature (see Fig. 3). It is for this reason that we take $\theta = 1.02\pi$. Although the local Berry curvature is no longer singular, the region of significant local Berry curvature is still very localized. This allows for a great degree of control of the amount of Berry curvature affecting the wave packet.

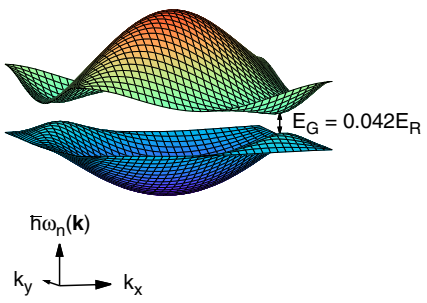


FIG. 2. (Color online) Energy spectrum of the first two bands. When $\theta = 1.02\pi$, a band gap with a size of $E_G = 0.042E_R$ is opened at the two Dirac points, where the two bands meet when $\theta = \pi$.

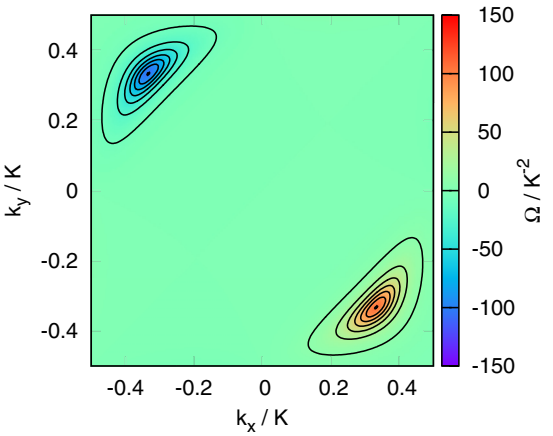


FIG. 3. (Color online) Local Berry curvature of the lowest band ($n = 1$). The $x$ and $y$ axes give the location in the Brillouin zone, while the color denotes the value of the local Berry curvature.

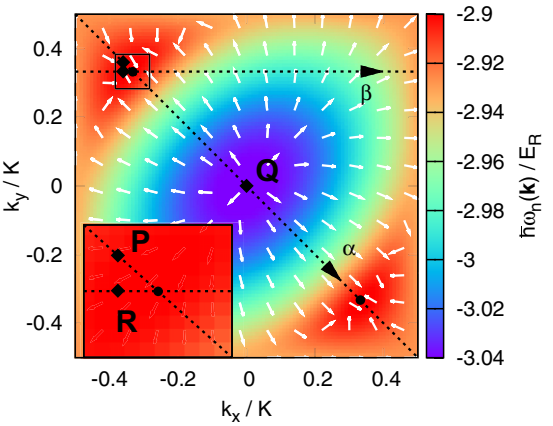


FIG. 4. (Color online) Two paths, $\alpha$ and $\beta$, in the first energy band ($n = 1$). The direction of the energy gradient, which is proportional to the local group velocity, is shown with the vector field. Both paths pass through at least one of the Dirac points, shown with black dots. For the diagonal path, $\alpha$, which is highly symmetric, the local group velocity is always aligned with the path; for the horizontal path, $\beta$, this is not so. Three trajectories with different starting points (indicated by black diamonds) are discussed here. In the first one, the wave packet is prepared at point **P** and travels along $\alpha$ in the direction indicated by the arrow. In the second one, the wave packet is prepared at **Q** and takes the same path. In the last trajectory, the wave packet starts at **R** and travels along $\beta$. The inset magnifies the region near **P** and **R** to clarify the difference between the two.

The results shown in Figs. 2–4 are found by numerical diagonalization of the unperturbed Hamiltonian. We combine this method with the approach described by Lax [36] to construct Berry connections and Bloch functions periodic in $\mathbf{k}$, which are used for the semianalytical approximation discussed next.

### B. Semianalytical approximation

For the envelope function in Eq. (9) we will use a Gaussian with a spread $\sigma = 0.05K$,

$$f_N(\mathbf{k}) = \frac{1}{\sqrt{\pi}\sigma} \exp\left(-\frac{(\mathbf{k}-\mathbf{k_0})^2}{2\sigma^2}\right), \tag{46}$$

where $\mathbf{k_0}$ is the mean of the envelope function. Initially, the wave packet is entirely in the first band, that is, $N = 1$. To study the evolution of the wave packet, a force of magnitude $F = \tilde{F}K E_R$ will be applied, where $\tilde{F} = 1/2000$ is a dimensionless parameter. With the application of a constant force, the wave packet travels in a straight line through the Brillouin zone. As described in Fig. 4, we will consider three trajectories that pass through at least one of the Dirac points where the band gap is the smallest and local Berry curvature the strongest. This allows the wave packet to exhibit more noticeable oscillations associated with the dynamical inverse effective-mass tensor and the dynamical anomalous velocity.

It is natural to decompose the full expression for the expectation value of the velocity of the wave packet in the same manner as Eq. (27),

$$\langle \hat{\mathbf{v}}(t)\rangle \approx \langle \mathbf{v}^{\mathrm{g}}(t)\rangle + \langle \mathbf{v}^{\mathrm{an}}(t)\rangle + \langle \mathbf{v}^{\mathrm{osc}}(t)\rangle, \tag{47}$$

where each of the three terms is an integration of $v_N^{\mathrm{g},a}(\mathbf{k})$, $v_N^{\mathrm{an},a}(\mathbf{k})$, and $\mathcal{V}_N^a(\mathbf{k},t)$ over the wave packet, respectively. In our first example we start with a wave packet at point $\mathbf{P}$ and a force in the direction of path $\alpha$ (see Fig. 4). The decomposition above is shown in Fig. 5. The dashed line corresponds to $\langle \mathbf{v}^{\mathrm{g}}(t)\rangle + \langle \mathbf{v}^{\mathrm{an}}(t)\rangle$, where both the group velocity and the anomalous velocity are taken into account. The solid line gives the full expression for $\langle \hat{\mathbf{v}}(t)\rangle$, with the oscillation term included. As expected from the discussion in Sec. III, at $t = 0$, the full expression for the velocity coincides with the prediction by just the group velocity. For $t > 0$, the velocity oscillates around the sum of the group and anomalous velocities. Within a tenth of the Bloch period these oscillations decay, but they reappear near the end of the Bloch oscillation.

Because of the high symmetry of path $\alpha$, the group velocity in this example is directed entirely along the direction of the force. This offers the closest analogy to a one-dimensional lattice [18]. To further explore this analogy, we decompose the dynamical oscillation term $\langle \mathbf{v}^{\mathrm{osc}}(t)\rangle$ into components parallel and orthogonal to the applied force [$\langle v_{\parallel}^{\mathrm{osc}}(t)\rangle$ and $\langle v_{\perp}^{\mathrm{osc}}(t)\rangle$, respectively; see Fig. 6].

The local anomalous velocity is derived from the cross product of the local Berry curvature with the force, and therefore, it is orthogonal to the force; similarly, the oscillating term associated with the anomalous velocity is also perpendicular to the force. Thus, the whole contribution to the parallel component of the dynamical oscillation of the velocity comes from oscillations of the group velocity. Interestingly, the converse is not true. Even though for this trajectory the group velocity is strictly parallel to the force so that the acceleration predicted simply by the inverse effective-mass tensor would be in that direction, the dynamical oscillation associated with the group velocity is not confined to this direction for $t > 0$. In fact, the dynamical oscillations in both $\mathbf{V}^{\mathrm{g}}(t)$ and $\mathbf{V}^{\mathrm{an}}(t)$ [see Eqs. (36) and (37)] contribute in the direction orthogonal to the force (see Fig. 6). Thus, even for highly symmetric paths, there can be oscillations of the velocity perpendicular to the force that are associated with the group velocity, so the strict analogy to motion in a one-dimensional lattice breaks down.

Both the group velocity and anomalous velocity are periodic because they depend only on properties of the band structure, which is periodic. However, the last term of Eq. (47), which is associated with $\mathcal{V}_N^a(\mathbf{k},t)$, is also dependent on the dynamics of the wave packet itself. As such, the full expression for velocity

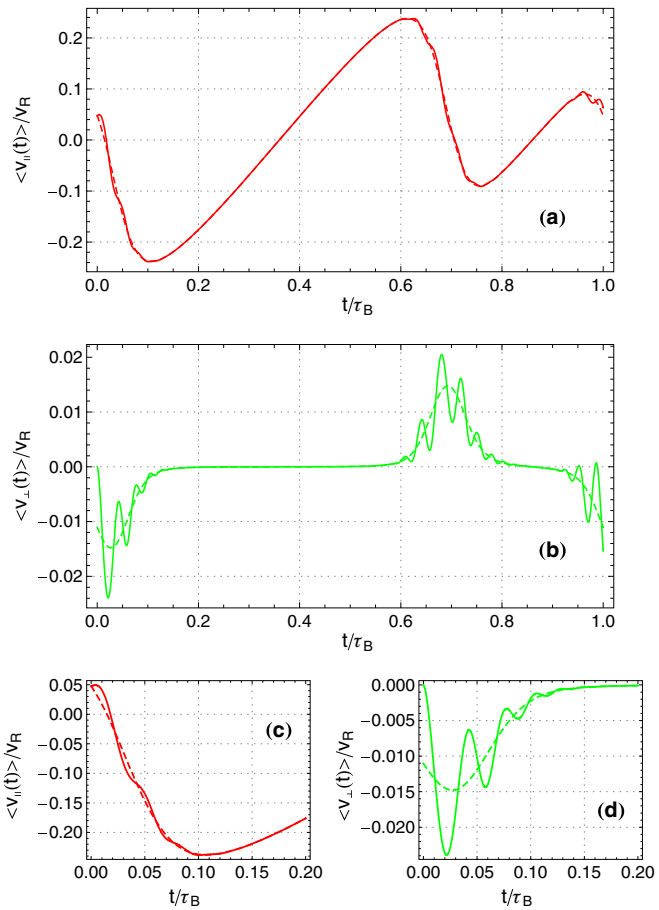


FIG. 5. (Color online) Expectation value of the velocity from the semianalytical approximation, Eq. (47), without the oscillating term $\langle \mathbf{v}^{\mathrm{osc}}(t)\rangle$ (dashed lines) and including it (solid lines). In this example the force points in the $(\hat{\mathbf{x}} - \hat{\mathbf{y}})/\sqrt{2}$ direction with $\tilde{F} = 1/2000$; the wave packet moves through the Brillouin zone starting at point $\mathbf{P}$ and following path $\alpha$ (see Fig. 4). The red curves correspond to $\langle \mathrm{v}_{\parallel}(t)\rangle$, the component of the velocity parallel to the force, while the green curves correspond to $\langle \mathrm{v}_{\perp}(t)\rangle$, the component of the velocity perpendicular to the force [$(\hat{\mathbf{x}} + \hat{\mathbf{y}})/\sqrt{2}$ direction]. Note that $\langle \mathbf{v}^{\mathrm{g}}(t)\rangle$ and $\langle \mathbf{v}^{\mathrm{an}}(t)\rangle$ only contribute to the parallel and perpendicular directions, respectively. (a) and (b) Results over one Bloch period, $\tau_B = \hbar K/F$. (c) and (d) Initial behavior of the velocity, showing the oscillations due to $\langle \mathbf{v}^{\mathrm{osc}}(t)\rangle$.

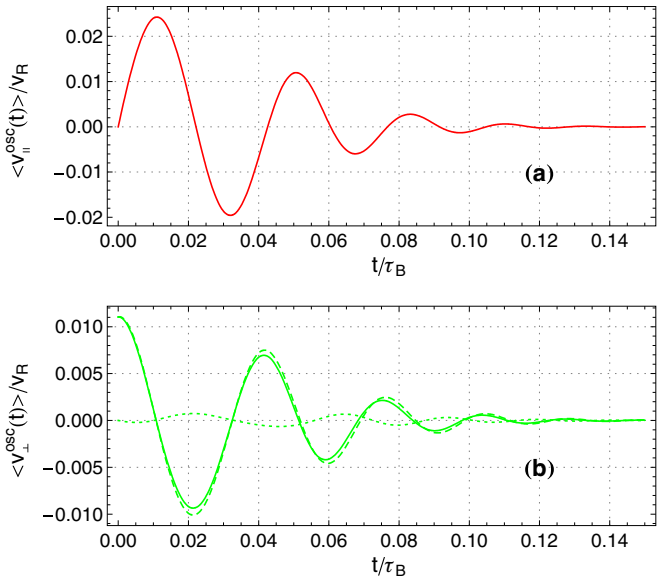


FIG. 6. (Color online) Decomposition of the oscillating term $\langle \mathbf{v}^{\rm osc}(t)\rangle$ (solid lines) into group velocity and anomalous velocity contributions for the example shown in Fig. 5; the curve in (a) corresponds to the parallel component of the velocity, and the curves in (b) correspond to the perpendicular components. In the direction parallel to the force, only the dynamical oscillations from $\mathbf{V}_N^{\rm g}(t)$ contribute. However, in the perpendicular direction both the dynamical oscillations from $\mathbf{V}_N^{\rm g}(t)$ (dotted line) and the dynamical oscillations from $\mathbf{V}_N^{\rm an}(t)$ (dashed line) contribute; the latter has a more significant contribution in the time range shown here.

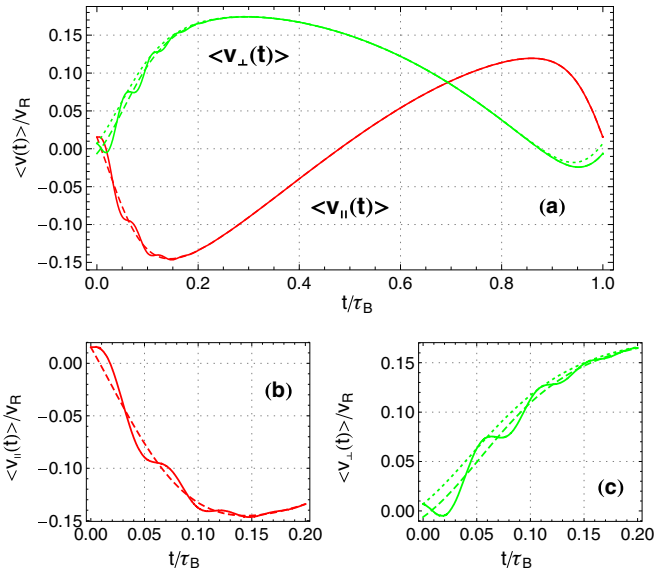


FIG. 8. (Color online) Expectation value of the velocity from the semianalytical approximation, Eq. (47), without the oscillating term $\langle \mathbf{v}^{\rm osc}(t)\rangle$ (dashed lines) and including it (solid lines). In this example the force points in the $\hat{\mathbf{x}}$ direction with $\tilde{F} = 1/2000$; the wave packet moves through the Brillouin zone starting at point $\mathbf{R}$ and following path $\beta$ (see Fig. 4). The red (dark gray) curves correspond to $\langle \mathrm{v}_\parallel(t)\rangle$, the component of the velocity parallel to the force, while the green (light gray) curves correspond to $\langle \mathrm{v}_\perp(t)\rangle$, the component of the velocity perpendicular to the force ($\hat{\mathbf{y}}$ direction). For reference, the component of the group velocity perpendicular to the force is plotted with dotted green lines. (a) Results over one Bloch period, $\tau_B = \sqrt{2}\hbar K/F$. (b) and (c) Initial behavior of the velocity, showing the oscillations due to $\langle \mathbf{v}^{\rm osc}(t)\rangle$.

does not exhibit periodicity. This dependence on the dynamics of the wave packet is even more evident when we change the starting point of the trajectory; for example, in Fig. 7 we choose $\mathbf{Q}$ to be the starting point, but we keep the force in the same direction so that the wave packet moves along path $\alpha$ (see Fig. 4). In this case the wave packet "experiences" the least amount of Berry curvature at the beginning (see Figs. 3 and 7). We see that the group and anomalous velocities are shifted as expected due to the new starting point; the dynamical oscillations in $\mathbf{V}^{\rm g}(t)$ and $\mathbf{V}^{\rm an}(t)$, on the other hand, have

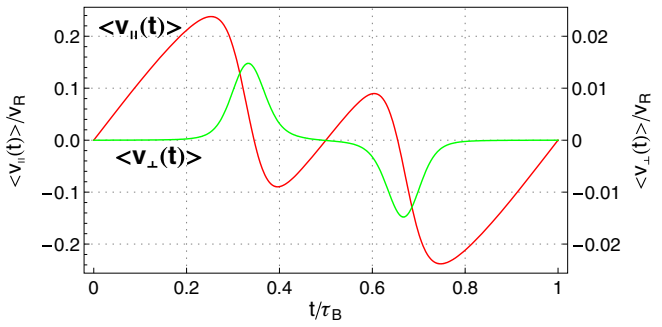


FIG. 7. (Color online) Expectation value of the velocity from the semianalytical approximation for the same parameters as in Fig. 5, but using $\mathbf{Q}$ as the starting point for the wave packet (see Fig. 4); the red (dark gray) curve corresponds to the parallel component of the velocity, and the green (light gray) curve corresponds to the perpendicular component of the velocity.

virtually vanished. From this observation, we conclude that the dynamical oscillations depend on the starting point of the wave packet, even when following the same path.

For the last example, shown in Figs. 8 and 9, we present a more general path without the symmetries of path $\alpha$. Starting at point $\mathbf{R}$, we direct the force parallel to path $\beta$ (see Fig. 4). Unlike in path $\alpha$, here the group velocity does not point exclusively along the direction of the force. The initial behavior shown in Fig. 8 is similar to what was seen in the first example. The velocity starts at the group velocity [dashed line for $\langle \mathrm{v}_\parallel(t)\rangle$ and dotted line for $\langle \mathrm{v}_\perp(t)\rangle$] and oscillates about the combination of the group and anomalous velocities (dashed lines). Despite not being strictly periodic, the dynamical oscillations of the velocity of the wave packet in path $\alpha$ were repetitive, at least qualitatively; we observed dynamical oscillations of similar amplitude and frequency at the start and the end of the Bloch oscillation. This is no longer true in the present example. After the initial dynamical oscillations of the velocity, no more revivals are seen near the end of the first Bloch oscillation; even during the second Bloch period, the dynamical oscillations are completely absent (see Fig. 11). This lack of revivals can be described as a form of dephasing. The tensor $\mathcal{J}_N^{ab}(\mathbf{k},t)$, which is responsible for the oscillations, contains a phase $\gamma_{nN}(\boldsymbol{\kappa},t)$ [see Eq. (28)]. This tensor is integrated over the wave packet as it moves through the Brillouin zone. In general, the phase in $\mathcal{J}_N^{ab}(\mathbf{k},t)$ accumulated

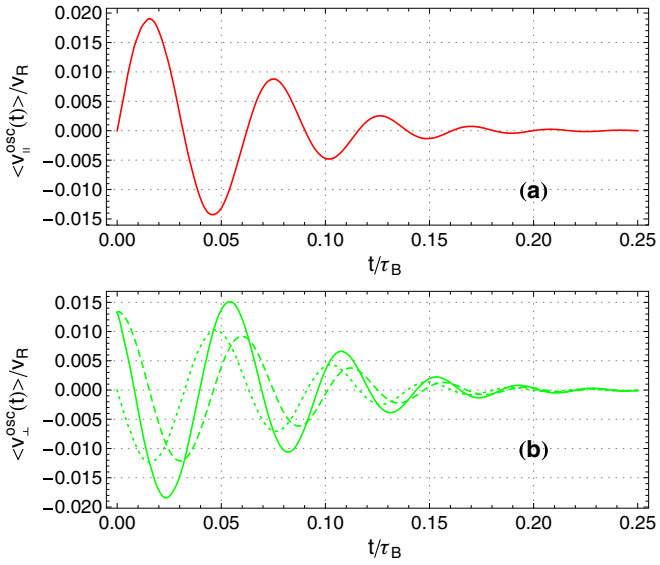


FIG. 9. (Color online) Decomposition of the oscillating term $\langle \mathbf{v}^{\rm osc}(t)\rangle$ (solid lines) into its group velocity and anomalous velocity contributions for the example shown in Fig. 8; the curve in (a) corresponds to the parallel component of the velocity, and the curves in (b) correspond to the perpendicular components of the velocity. In the direction parallel to the force, only the dynamical oscillations from $\mathbf{V}_N^{\rm g}(t)$ contribute. However, in the perpendicular direction, both the dynamical oscillations from $\mathbf{V}_N^{\rm g}(t)$ (dotted line) and the dynamical oscillations from $\mathbf{V}_N^{\rm an}(t)$ (dashed line) contribute; in contrast to the behavior in Fig. 6, the two types of oscillations make similar contributions to $\langle \mathbf{v}^{\rm osc}(t)\rangle$.

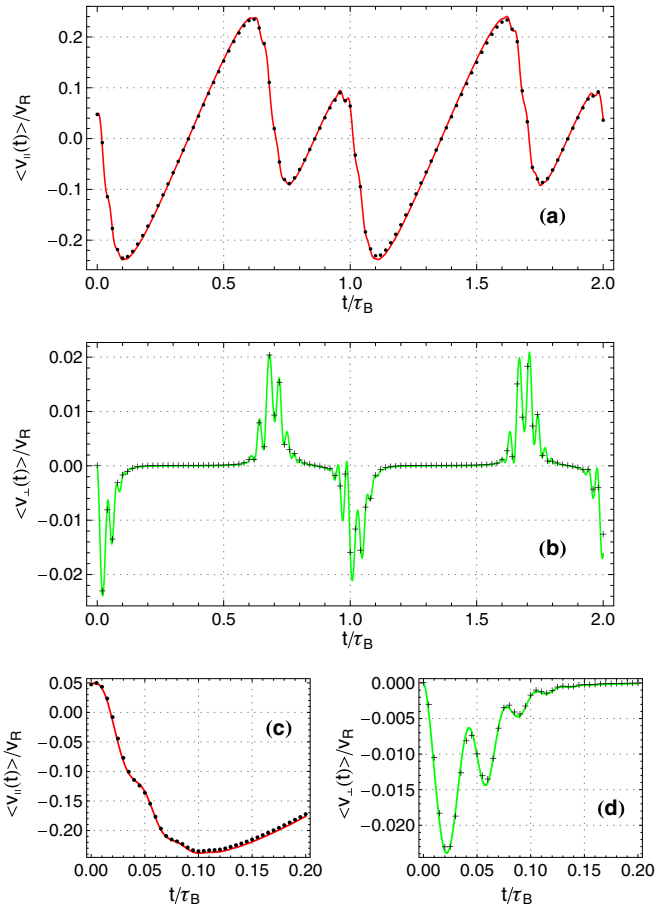


FIG. 10. (Color online) Comparison between the expectation value of the velocity shown in Fig. 5 for path $\alpha$ in the Brillouin zone (solid lines) and a full numerical calculation (dots and crosses). The red lines and black dots correspond to the components of the velocity parallel to the force; the green lines and black crosses correspond to the components of the velocity perpendicular to the force. (a) and (b) Results over two Bloch periods. (c) and (d) Initial behavior of the velocity, showing the oscillations due to $\langle \mathbf{v}^{\rm osc}(t)\rangle$ [see Eq. (47)].

by each $\mathbf{k}$ component of the wave packet can be different even after a full Bloch period, and we expect to observe dephasing. For the central path $\alpha$, however, the $\mathbf{k}$ components of the wave packet trace pairs of parallel paths that are reflections of each other along the diagonal and acquire the same phase; therefore, with respect to the dephasing, the motion for path $\alpha$ is essentially the same as in the one-dimensional case, where revivals are observed [18]. This kind of symmetry is not seen for a wave packet moving along the central path $\beta$, which explains why the oscillations decay in this case.

### C. Comparison with full numerical solutions

In order to verify the validity of the semianalytical results presented in Sec. IV B, we compare them with full numerical solutions of the time-dependent Schrödinger equation for the Hamiltonian (3), with a force suddenly applied at $t = 0$ and left constant afterwards. For the full numerical calculation we use the split-step-operator method [43]. As usual, the kinetic-energy term of the Hamiltonian is treated in Fourier space, the potential-energy term (including the applied force) is treated in real space, and we switch back and forth between the two spaces with a fast-Fourier-transform implementation [44]. The expectation value of the velocity is calculated from the Fourier components of the wave packet.

In Figs. 10 and 11 we compare the expectation value of the velocity for paths $\alpha$ and $\beta$ in the Brillouin zone presented in Figs. 5 and 8 with full numerical calculations over two Bloch periods. Note the excellent agreement between the two approaches over short and long time scales. The force used in these examples is small enough to guarantee that the semianalytical expression (27) predicts correctly the oscillations associated with the dynamics of the effective mass and anomalous transport. Furthermore, the presence of revivals for path $\alpha$ (see Fig. 10) and their absence for path $\beta$ (see Fig. 11) are confirmed by the full numerical calculation.

We can also illustrate the evolution of the wave packet in real space using the results from the time propagation with the split-step-operator method. In Fig. 12 we show snapshots of the wave packet in the two situations considered in Figs. 10 and 11 for different times within one Bloch period. In both cases the initial wave packets are the same, but over time the trajectory (dashed line in Fig. 12) and dispersion of the wave packets evolve differently. Due to the symmetry of path $\alpha$ (see Fig. 4), the group velocity is always parallel or antiparallel to the force, resulting in an oscillation along that direction [see Figs. 12(a)–12(e)]. On the other hand, for path $\beta$, the wave packet traces a more complicated trajectory in real space, and it does not return to its starting point [see Figs. 12(f)–12(j)].

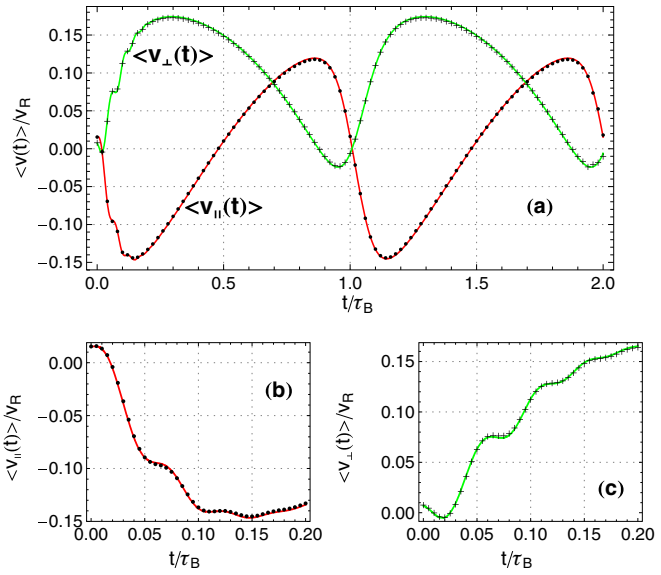


FIG. 11. (Color online) Comparison between the expectation value of the velocity shown in Fig. 8 for path $\beta$ in the Brillouin zone (solid lines) and a full numerical calculation (dots and crosses). The red lines and black dots correspond to the components of the velocity parallel to the force; the green lines and black crosses correspond to the components of the velocity perpendicular to the force. (a) Results over two Bloch periods. (b) and (c) Initial behavior of the velocity, showing more clearly the oscillations due to $\langle \mathbf{v}^{\mathrm{osc}}(t)\rangle$ [see Eq. (47)].

The anomalous velocity and the dynamical corrections modify the real-space trajectories described by the group velocity alone, but this change is small compared with the scale of the trajectories shown in Fig. 12 over one Bloch period. With respect to the dispersion of the wave packet, the spread is more pronounced for path $\beta$ than for path $\alpha$ [compare Figs. 12(c) and 12(h)], and the shape of the wave packet remains more symmetric around its center for path $\alpha$ [compare Figs. 12(c)–12(e) and 12(h)–12(j)].

The ultimate breakdown of the semianalytical expression (27) is associated with Zener tunnelling, the probability of which increases for larger forces. Wannier's method of decoupling the bands in the presence of an applied force [22] cannot describe Zener tunneling even if higher orders of his power expansion are considered [20]. Accordingly, the picture presented in Sec. II is valid only for wave packets mainly in one band with small amplitudes over neighboring bands, which is the typical requirement in the semiclassical description of transport. The start of the breakdown of the semianalytical approximation is shown in Fig. 13 for path $\alpha$ (see Fig. 4) and a force twice as large as the one used so far. In this case the most significant difference between the semianalytical approximation and the full numerical calculation appears in the component of the velocity parallel to the force, as the semianalytical result overestimates the amplitude of the Bloch oscillation of the usual group velocity. This deviation occurs early in the evolution of the expectation value of the velocity since the starting point of the trajectory in the Brillouin zone is near one of the Dirac points, where the first two bands are close and Zener tunneling is more probable. Nevertheless, note that Eq. (27) is still a good approximation, as it agrees at least qualitatively with the full numerical calculation.

In the semianalytical approximation the wave packet $|\Psi(t)\rangle$ is a superposition of a main MBS wave packet associated with

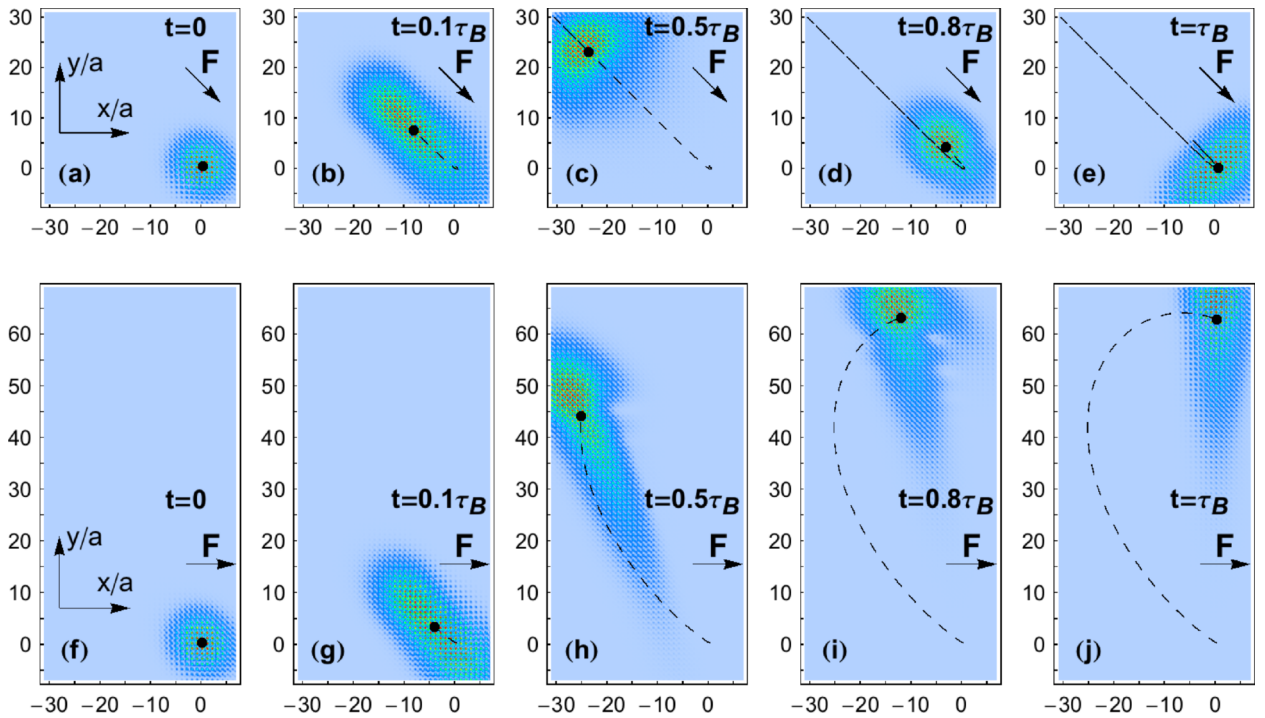


FIG. 12. (Color online) Time evolution of the absolute value of the wave packet in real space calculated using the split-step-operator method for (a)–(e) path $\alpha$ and (f)–(j) path $\beta$ in the Brillouin zone. The parameters are the same as the ones used in Figs. 10 and 11. The black dots mark the expectation value of the position for the snapshot time, and the dashed line shows the trajectory starting at $t = 0$. The horizontal and vertical axes show the position in units of the lattice constant.

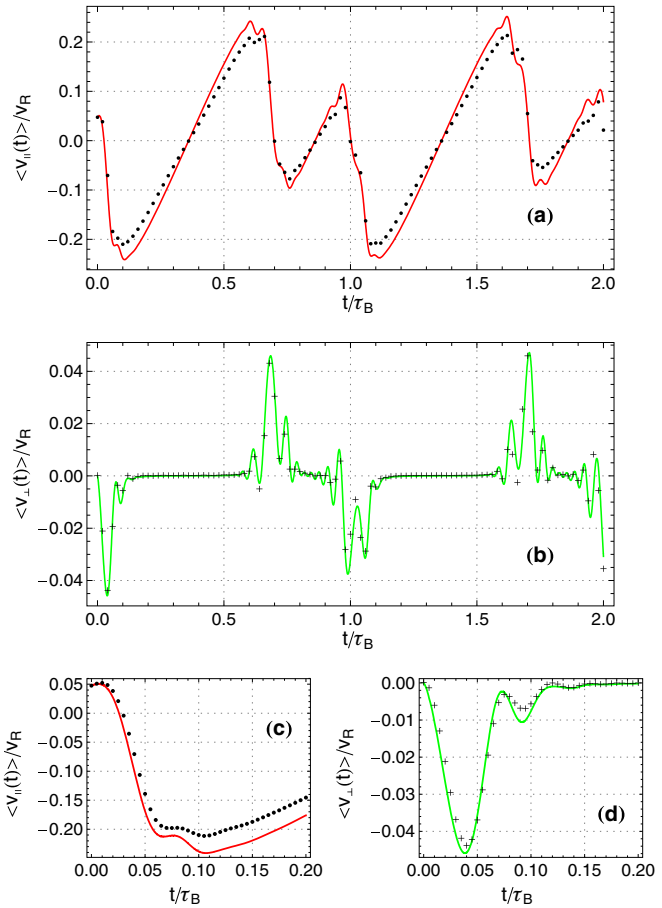


FIG. 13. (Color online) Comparison between the semianalytical approximation (solid lines) and the full numerical calculation (dots and crosses) for the same parameters as in Fig. 5, but doubling the force ($\tilde{F} = 1/1000$). The red lines and black dots correspond to the components of the velocity parallel to the force; the green lines and black crosses correspond to the components of the velocity perpendicular to the force. (a) and (b) Results over two Bloch periods. (c) and (d) Initial behavior of the velocity, showing the oscillations due to $\langle \mathbf{v}^{\mathrm{osc}}(t) \rangle$ [see Eq. (47)].

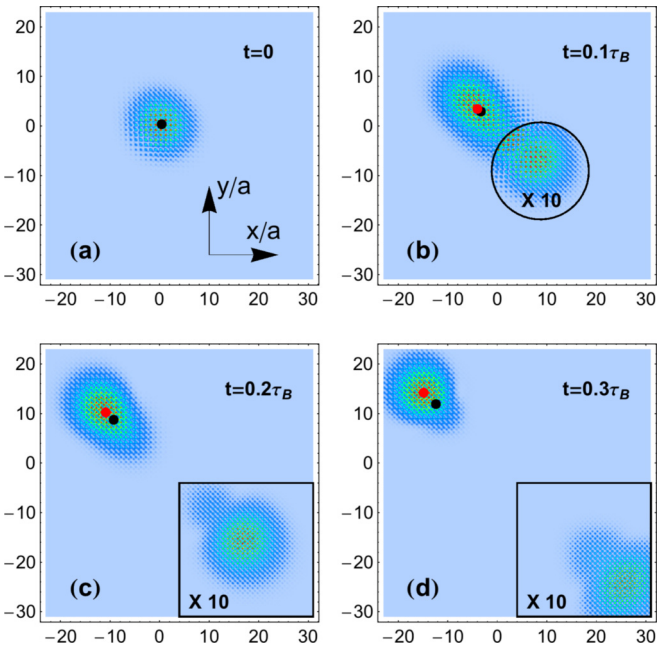


FIG. 14. (Color online) Snapshots of the absolute value of the wave packet for the parameters used in Fig. 13 calculated from the time evolution using the split-step-operator method. At $t = 0.1\tau_B$, a wavelet starts to form, and afterwards it moves towards the lower right corner of the real-space window. The black and red (gray) dots mark the expectation value of the position for the snapshot time, calculated from the full numerical and semianalytical calculations, respectively. In (b)–(d) the smaller frames show the absolute value of the wave packet amplified ten times. The horizontal and vertical axes show the position in units of the lattice constant.

band $N$ [see Eq. (25)] and MBS wave packets with smaller amplitudes associated with neighboring bands, $n \neq N$ [see Eq. (26)]. This suggests that the initial wave packet in real space will split into a main wave packet associated with band $N$ and small ones associated with $n \neq N$; these wave packets will move differently according to the properties of the band to which they correspond. The presence of this splitting is confirmed by the full numerical calculation, as illustrated in Fig. 14 for the parameters used in Fig. 13. The snapshots in Fig. 14 show a main wave packet associated with band $N = 1$ and a small wave packet associated with the next band, $n = 2$, which moves in the direction opposite that of the main wave packet.

Even though the semianalytical approximation predicts the splitting of the initial wave packet, it cannot describe correctly the amplitude and shape of the small wave packet for strong forces, such as the one used in Fig. 14. The failure of the semianalytical approach in this example is shown in Fig. 15, where we compare the wave packets calculated using this approximation and the results from the full numerical calculation. Note that the main wave packet is essentially the same in the two approaches [compare Figs. 15(a) and 15(b)], but the semianalytical result predicts a small wave packet with a different shape and underestimates its amplitude [compare Figs. 15(c) and 15(d)]. Consequently, the expectation value of the position differs in the two calculations, which can be seen in Figs. 14 and 15, where the expectation value of the position calculated with the semianalytical approximation [red (gray) dots] is shifted in the direction of the small wave packet for the full numerical calculation (black dots). The incorrect description of the small wave packet by the semianalytical approximation is responsible for the overestimation of the group velocity calculated with this method in Fig. 13. As the applied force is increased, Zener tunneling becomes more important, and the amplitudes of the wave packets associated with the neighboring bands, $n \neq N$, increase; consequently, the weight of these amplitudes modifies more significantly the expectation values of position and velocity predicted by the main wave packet alone. Since the semianalytical approximation cannot predict correctly the contribution of these wave packets, the dynamics calculated with this approach become less accurate.

## V. CONCLUSION

We have discussed the dynamics of a wave packet in a periodic potential prepared in one band and subject to

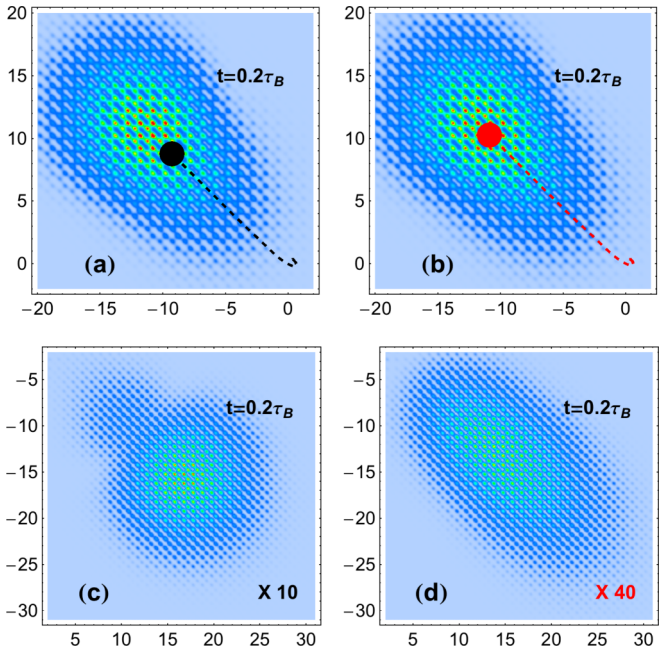


FIG. 15. (Color online) Detailed view of the wave packet shown in Fig. 14(c). The black and red (gray) dots (and the dashed lines) mark the expectation value of the position calculated from the full numerical and semianalytical calculations, respectively. The horizontal and vertical axes show the position in units of the lattice constant. (a) and (b) Main wave packet from the full numerical and semianalytical calculations, respectively. (c) and (d) Small wave packet from the full numerical and semianalytical calculations, respectively.

the sudden application of a uniform force, which remains constant afterwards. We have found that the usual semiclassical description, involving the inverse effective-mass tensor and the anomalous velocity, requires corrections. When the force is suddenly applied, the particle responds initially as if it were free; its acceleration is characterized by the bare mass [see Eq. (44)], and there is no anomalous velocity [see Eq. (43)]. However, it is possible to define dynamical quantities associated with the inverse effective-mass tensor [see Eq. (39)] and the anomalous velocity [see Eq. (38)]. These quantities initially take the values that would characterize a free particle; at later times they oscillate about the usual expressions for these quantities as the wave packet moves through the Brillouin zone. The total velocity of the wave packet, Eq. (35), includes a dynamical group velocity, which is associated with the dynamical inverse effective-mass tensor, and the aforementioned dynamical anomalous velocity. Even for cases when the usual inverse effective-mass tensor predicts an acceleration parallel to the applied force (for example, in path $\alpha$ in Fig. 4), the dynamical inverse effective-mass tensor allows for oscillations of the velocity parallel and perpendicular to the force (see Fig. 6). In addition to the acceleration described by the dynamical inverse effective-mass tensor, there is a dynamical anomalous acceleration associated with the dynamical anomalous velocity [see Eq. (41)]; both of these dynamical anomalous quantities are always perpendicular to the applied force.

We have derived semianalytic expressions for all of these dynamical quantities and have calculated them for a particle subject to a suddenly applied force in a two-dimensional optical lattice [23]. Besides exhibiting aspects of wave-packet motion involving the topology of the bands, which do not arise in one-dimensional lattices, the wave-packet motion in the two-dimensional lattice shows interesting features in the interplay between the Bloch oscillations and the dynamics of the group and anomalous velocities. In one-dimensional lattices it was shown that the initial dynamical oscillations have revivals after a Bloch period as a result of the cyclic path of the wave packet in the Brillouin zone [18]. In the two-dimensional lattice considered here, we showed that not every cyclic path in the Brillouin zone leads to revivals after one Bloch period (see Fig. 11); these revivals only occur for paths where the symmetry of the band structure allows each **k** component of the wave packet to accumulate similar phases over a Bloch period (see Fig. 10). This behavior shows that, while the group velocity and the Berry curvature have a periodicity given by the Bloch period, the dynamical oscillations discussed here do not display such periodicity. Revivals are still possible in the two-dimensional lattice for some paths, but the dynamical oscillations are still not periodic over one Bloch period. Furthermore, these oscillations depend on the starting location on the chosen path in the Brillouin zone (compare Figs. 5 and 7).

The results from the semianalytical approximation were confirmed by a full numerical solution of the dynamics of the wave packet. The agreement breaks down for strong forces due to the limitations of the modified Bloch states to decouple completely the bands in the presence of an applied force [20]. In real space the wave packet splits into a main wave packet, associated with the original initial band, and a small wave packet, associated with the next neighboring band (see Fig. 14); the semianalytical approximation fails to capture correctly the amplitude and shape of the small wave packet, affecting the expectation values of position and velocity calculated with this method (see Fig. 15). However, since the main wave packet is well described by the semianalytical approximation, we find that even for a strong force the prediction of the dynamical oscillations given by this approximation is at least qualitatively correct (see Fig. 13).

Two-dimensional optical lattices are readily available, suggesting that the dynamics described here can be observed experimentally in this type of system; this would generalize and extend the recent experimental study of these dynamics in a one-dimensional optical lattice [19]. For the application of a force to be "sudden," the time scale of its appearance must be short compared with the time associated with the energy difference between the band of the initial wave packet and the nearest neighboring band. In solid-state systems the time scales and the difficulties in controlling the properties of the lattice have prohibited the observation of the dynamical inverse effective-mass tensor, even though some deviations from the usual effective-mass behavior have been attributed to its dynamical oscillations [31]; nonetheless, attosecond science is pushing the time scales for which carrier dynamics in solids can be observed to the subfemtosecond regime [32–34]. We believe that these developments, combined with the growing interest in topological properties of periodic potentials and their dynamical consequences [10,30,45–47],

make the oscillations discussed here an interesting phenomenon to study experimentally in both optical lattices and solid-state systems.

**ACKNOWLEDGMENT**

This work was supported by the Natural Sciences and Engineering Research Council of Canada (NSERC).

[1] N. W. Ashcroft and N. D. Mermin, *Solid State Physics* (Saunders College, Philadelphia, 1976).
[2] D. J. Thouless, M. Kohmoto, M. P. Nightingale, and M. den Nijs, Phys. Rev. Lett. **49**, 405 (1982).
[3] M. V. Berry, Proc. R. Soc. London, Ser. A **392**, 45 (1984).
[4] B. Simon, Phys. Rev. Lett. **51**, 2167 (1983).
[5] M. Z. Hasan and C. L. Kane, Rev. Mod. Phys. **82**, 3045 (2010).
[6] R. Karplus and J. M. Luttinger, Phys. Rev. **95**, 1154 (1954).
[7] E. Adams and E. Blount, J. Phys. Chem. Solids **10**, 286 (1959).
[8] G. Sundaram and Q. Niu, Phys. Rev. B **59**, 14915 (1999).
[9] N. A. Sinitsyn, J. Phys.: Condens. Matter **20**, 023201 (2008).
[10] D. Xiao, M.-C. Chang, and Q. Niu, Rev. Mod. Phys. **82**, 1959 (2010).
[11] Y. D. Chong, Phys. Rev. B **81**, 052303 (2010).
[12] E. N. Adams, Phys. Rev. **107**, 698 (1957).
[13] A. Nenciu, J. Phys. A **41**, 025304 (2008).
[14] D. Pfirsch and E. Spenke, Z. Phys. **137**, 309 (1954).
[15] J. B. Krieger and G. J. Iafrate, Phys. Rev. B **35**, 9644 (1987).
[16] K. Hess and G. Iafrate, Proc. IEEE **76**, 519 (1988).
[17] G. J. Iafrate, J. P. Reynolds, J. He, and J. B. Krieger, Int. J. High Speed Electron. Syst. **9**, 223 (1998).
[18] F. Duque-Gomez and J. E. Sipe, Phys. Rev. A **85**, 053412 (2012).
[19] R. Chang, S. Potnis, R. Ramos, C. Zhuang, M. Hallaji, A. Hayat, F. Duque-Gomez, J. E. Sipe, and A. M. Steinberg, Phys. Rev. Lett. **112**, 170404 (2014).
[20] G. Nenciu, Rev. Mod. Phys. **63**, 91 (1991).
[21] E. N. Adams and P. N. Argyres, Phys. Rev. **102**, 605 (1956).
[22] G. H. Wannier, Phys. Rev. **117**, 432 (1960).
[23] L. Tarruell, D. Greif, T. Uehlinger, G. Jotzu, and T. Esslinger, Nature (London) **483**, 302 (2012).
[24] O. Morsch and M. Oberthaler, Rev. Mod. Phys. **78**, 179 (2006).
[25] M. Aidelsburger, M. Atala, S. Nascimbène, S. Trotzky, Y.-A. Chen, and I. Bloch, Phys. Rev. Lett. **107**, 255301 (2011).
[26] G.-B. Jo, J. Guzman, C. K. Thomas, P. Hosur, A. Vishwanath, and D. M. Stamper-Kurn, Phys. Rev. Lett. **108**, 045305 (2012).
[27] A. M. Dudarev, R. B. Diener, I. Carusotto, and Q. Niu, Phys. Rev. Lett. **92**, 153005 (2004).
[28] G. Pettini and M. Modugno, Phys. Rev. A **83**, 013619 (2011).
[29] H. M. Price and N. R. Cooper, Phys. Rev. A **85**, 033620 (2012).
[30] G. Jotzu, M. Messer, R. Desbuquois, M. Lebrat, T. Uehlinger, D. Greif, and T. Esslinger, arXiv:1406.7874.
[31] Y. M. Zhu, T. Unuma, K. Shibata, K. Hirakawa, Y. Ino, and M. Kuwata-Gonokami, Phys. Status Solidi C **5**, 240 (2008).
[32] S. Ghimire, A. D. DiChiara, E. Sistrunk, P. Agostini, L. F. DiMauro, and D. A. Reis, Nat. Phys. **7**, 138 (2011).
[33] M. Isanov and O. Smirnova, Chem. Phys. **414**, 3 (2013).
[34] O. Schubert, M. Hohenleutner, F. Langer, B. Urbanek, C. Lange, U. Huttner, D. Golde, T. Meier, M. Kira, S. W. Koch, and R. Huber, Nat. Photon. **8**, 119 (2014).
[35] E. I. Blount, in *Solid State Physics: Advances in Research and Applications*, edited by F. Seitz and D. Turnbull (Academic Press, New York, 1962), Vol. 13, p. 305.
[36] M. Lax, *Symmetry Principles in Solid State and Molecular Physics* (Wiley-Interscience, New York, 1974).
[37] In [22], Wannier also considers the generalization of his decoupling method to bands that share degenerate points. For simplicity, we assume nondegenerate bands throughout, an assumption that is valid in the type of potential considered in Sec. IV.
[38] Equation (2), or, equivalently, Eq. (14), is also used as a definition of the effective mass in other scenarios in solid-state physics, such as in the $\mathbf{k}\cdot\mathbf{p}$ method for calculating band structures [36].
[39] F. Bloch, Z. Phys. **52**, 555 (1929).
[40] This is strictly true if there are no degeneracies. For example, the two-dimensional hexagonal lattice with sixfold symmetry, which is characteristic of systems such as graphene, has singular local Berry curvature at the Dirac points where the two lowest bands touch (see [42]).
[41] The expression for the potential used here is the same as Eq. (1) in [23] after a $\pi/4$ rotation in the counterclockwise direction and replacing their laser wave vector $k$ by $K=\sqrt{2}k$; after this rotation the lattice vectors become horizontal and vertical. Additionally, since we choose $K$ instead of $k$ to define the recoil energy, our recoil energy is twice the one used in [23].
[42] J. N. Fuchs, F. Piéchon, M. O. Goerbig, and G. Montambaux, Eur. Phys. J. B **77**, 351 (2010).
[43] M. D. Feit, J. A. Fleck, Jr., and A. Steiger, J. Comput. Phys. **47**, 412 (1982).
[44] M. Frigo and S. G. Johnson, Proc. IEEE **93**, 216 (2005).
[45] K. S. Virk and J. E. Sipe, Phys. Rev. Lett. **107**, 120403 (2011).
[46] H. Murakawa, M. S. Bahramy, M. Tokunaga, Y. Kohama, C. Bell, Y. Kaneko, N. Nagaosa, H. Y. Hwang, and Y. Tokura, Science **342**, 1490 (2013).
[47] F. Yang and R.-B. Liu, New J. Phys. **15**, 115005 (2013).